Journal of Engineering Mathematics **42:** 157–180, 2002.

Buckling and collapse of open and closed cylindrical shells

C. POZRIKIDIS
Department of Mechanical and Aerospace Engineering; University of California, San Diego; La Jolla, CA 92093-0411, U.S.A; e-mail cpozrikidis@ucsd.edu

Received 9 May 2001; accepted in revised form 31 January 2002

Abstract. The buckling of a finite section of a cylindrical shell resembling a two-dimensional contact lens, and the collapse of a tubular shell of infinite extent are considered. The deformation is due, respectively, to the application of an edge force or to a negative transmural pressure. In both cases, the shell develops elastic bending moments due to the deformation from a specified resting shape according to a linear constitutive equation, accompanied by in-plane and transverse shear tensions. In the case of a section of a shell with a flat resting shape, classical results due to Euler and Love show that, as the applied edge force is increased beyond a sequence of thresholds, an infinite family of deformed shapes becomes possible corresponding to buckled states that bifurcate from the zero-curvature resting configuration. It is shown here that a corresponding infinite family of shapes is also possible for a finite shell whose resting shape is a section of circle. These shapes, however, no longer arise from bifurcations, but rather constitute disconnected solution branches of a nonlinear boundary-value problem. A closed cylindrical shell whose cross-section has a circular resting shape exhibits similar bifurcations when the difference between the exterior and interior pressure exceeds a sequence of thresholds, but a shell with a non-circular resting shape deforms into a multitude of shapes described by isolated solution branches. The computed two-dimensional buckled shapes are used to reconstruct the three-dimensional shape of a slowly collapsing fluid-conveying vessel. The reconstruction procedure involves stacking together cross-sections at axial positions that are found by integrating the differential equation determining the axial pressure distribution in unidirectional pressure-driven flow, subject to a constant flow rate. The dimensionless coefficient relating the local pressure gradient to the flow rate is computed by solving the Poisson equation governing unidirectional viscous flow using a boundary-element method, and expressing the flow rate as a boundary integral involving the shear stress which is available from the solution of the boundary-integral equation. In an appendix, the energy of the bending state is discussed with reference to specific choices made by previous authors in various branches of science and engineering.

Key words: bifurcation, boundary-value problems, collapsible tubes, eigenvalues, elastic shells.

1. Introduction

A variety of natural, biological and engineering systems involve thin sheets of a pure or composite elastic material, and sheet-like molecular networks classified as flexible shells. In the course of their intended function, the shells deform and may buckle under the influence of a localized or distributed load due to their weight, an applied system of forces and torques, an ambient or internal hydrostatic pressure, or a more general hydrodynamic traction. Deformation is accompanied by the development of stresses whose areal integrals over the cross-section are recognized as stress resultants or tensions. In the case of shells consisting of thin elastic sheets, the first moments of the stresses integrated over the cross-section amount to distributed bending moments. In the case of molecular networks, bending moments arises due to a preferred orientation of chemical bonds. Mathematical idealization reduces a thin shell to a material surface with infinitesimal thickness whose dynamics is described by the Lagrangian geometry of the deformed configuration relative to that in the unstressed state.

Fundamental studies of small and large shell deformations, respectively called buckling and post-bucking, can be traced back to the seminal works of Euler, von Kàrmàn and Love [1–3]. The importance of shell mechanics in oceanography, civil, aerospace, and structural engineering has spawn an immense body of literature including fundamental and applied studies of statics, dynamics, and stability (*e.g.* [4–6]). Part of the literature was motivated by the realization that the deformation of shells under mechanical load or due to flow-structure interaction is pertinent to a host of problems in materials science, chemical physics, biology, and biomechanics, and also by the discovery that post-buckling admits a complex solution space that can be successfully analyzed using modern tools of stability and bifurcation theory, where it even serves as a paradigm. For example, shell theory has been applied to describe the collapse of the endothelium surface of pulmonary and blood flow vessels such as bronchiols and veins [7], the deformation of biological membranes enclosing red blood cells and other vesicles [8], and the cockling (hygroscopic buckling) of paper [9]. Recently, Steigmann and Ogden considered the deformation of thin shells coated on the surfaces of elastic media and established a theoretical framework for the development of constitutive equations regarding the bending moments [10–12].

In this paper, we consider the deflection and post-buckling of open and closed (tubular) cylindrical shells with non-planar and non-circular cross-sectional resting shapes. Our main goal is to elucidate how the curvature of the resting shape of an open shell, and the non-uniformity of the curvature of a closed tubular shell affect the equilibrium shapes at small and large deformations. This issue has been discussed by numerous previous authors, but only in general terms and in the context of shape imperfection, as will be reviewed in subsequent sections.

In Section 2, we formulate the problem of two-dimensional shell deformation in terms of the curvature or slope angle of the shell contour in the deformed state, unify and discuss the merits of the two approaches, and derive some new results. In both cases, we obtain a boundary-value problem involving an unspecified parameter that is declared an eigenvalue. In Section 3, we consider the deformation of plates with flat and circular resting shapes, and illustrate explicitly the transition from double-point bifurcation in solution space to a solution structure involving disconnected loops. In Section 4, we consider the corresponding deformation of tubular shells with circular and non-circular resting shapes, and demonstrate a similar but more subtle behavior.

In Section 5, we consider fluid-carrying tubes collapsing due to a decrease in the internal pressure with streamwise position associated with a negative pressure gradient necessary to drive the flow, and develop a method of reconstructing the three-dimensional tube shape in terms of the available two-dimensional buckled profiles. The two-dimensional cross-sections are placed at axial positions that are computed by integrating the differential equation governing the axial pressure distribution subject to a constant flow rate. A dimensionless constant relating the local pressure gradient to the flow rate is found by solving the Poisson equation describing unidirectional flow along a tube with a collapsed profile using a boundary-integral method. A new result is an expression for the flow rate in pressure-driven flow through a tube with arbitrary cross-section in terms of the boundary distribution of the shear stress, which is available from the solution of the boundary-integral equation.

In Appendix A, we consider the energetics of the deformation, provide justification for the linear constitutive equation for the bending moments in terms of the curvature, and establish a framework for choices made by previous authors concerning the tensions and normal loads developing along macromolecules, slender bodies of fluid, and fluctuating membranes.

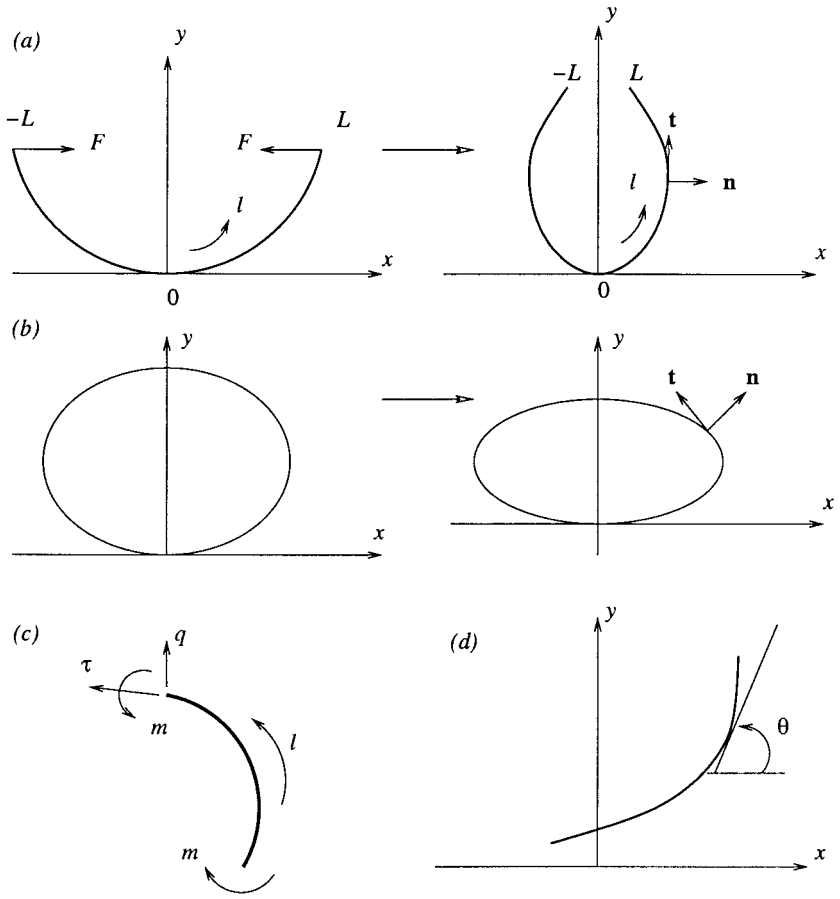

Figure 1. Illustration of (a) an open cylindrical shell resembling a two-dimensional contact lens, deforming under the action of an edge force; (b) a closed cylindrical shell deforming under the action of a pressure difference between the exterior and interior; (c, d) A section of the shell showing the in-plane and transverse shear tensions τ and q, the bending moment m, and the slope angle θ.

2. Problem statement and governing equations

We consider small and large deformations of open or closed cylindrical shells consisting of an elastic material. In the first problem, we consider the symmetric deformation of an open shell of finite extent due to a compressive force F applied at both ends, as illustrated in Figure 1(a), and seek to compute the shape that the shell assumes after the two ends have been displaced by a certain distance. Physically, the shell may be identified with a paper card or a two-dimensional optical contact lens pinched by two fingers at the two ends. In the second problem, we consider the buckling of an infinite tubular cylindrical shell, as illustrated in Figure 1(b), and seek to compute the shape that the shell assumes after a certain pressure difference between the exterior and interior has been applied.

2.1. Tensions, bending moments, and equilibrium

We begin formulating the governing equations by considering the shell in the deformed state, and identify point particles by the arc length l. In the case of the open shell depicted in

Figure 1(a), the arc length varies in the range $[-L, L]$, where $2L$ is the total arc length of the shell, an the origin has been placed at the mid-point. In the case of the closed shell depicted in Figure 1(b), the arc length varies in the range $[0, L]$, where L is the shell perimeter.

Because of the deformation, the shell develops an in-plane tension τ, a transverse shear tension q, and a bending moment m, as illustrated in Figure 1(c). The vectorial tension exerted on a cross-section is given by

$$\mathbf{T} = \tau\mathbf{t} + q\mathbf{n}, \tag{2.1}$$

where $\mathbf{t}$ is the unit tangent vector pointing in the direction of increasing arc length l, and $\mathbf{n}$ is the unit normal vector.

In the case of the open shell depicted in Figure 1(a), global equilibrium requires $\mathbf{T} = -F\mathbf{e}_x$, where $\mathbf{e}_x$ is the unit vector along the x axis. Under more general circumstances, a force balance requires

$$\frac{\mathrm{d}\mathbf{T}}{\mathrm{d}l} + \mathbf{p} = \frac{\mathrm{d}}{\mathrm{d}l}(\tau\mathbf{t} + q\mathbf{n}) + \mathbf{p} = \mathbf{0}, \tag{2.2}$$

where $\mathbf{p}$ is the distributed load due, for example, to hydrostatic pressure or a more general hydrodynamic traction. Expanding out the derivatives of the products on the left-hand side of (2.2), and using the relations

$$\frac{\mathrm{d}\mathbf{t}}{\mathrm{d}l} + \kappa\mathbf{n} = \mathbf{0}, \qquad \frac{\mathrm{d}\mathbf{n}}{\mathrm{d}l} - \kappa\mathbf{t} = \mathbf{0}, \tag{2.3}$$

where κ is the curvature of the shell in the xy plane, we obtain the normal and tangential force balances

$$-\kappa\tau + \frac{\mathrm{d}q}{\mathrm{d}l} = -\mathbf{p}\cdot\mathbf{n} \equiv -p_n, \qquad \kappa q + \frac{\mathrm{d}\tau}{\mathrm{d}l} = -\mathbf{p}\cdot\mathbf{t} \equiv -p_t. \tag{2.4}$$

In the case of the open shell depicted in Figure 1(a), p_t and p_n both vanish; in the case of the closed shell depicted in Figure 1(b), p_t vanishes but $p_n \equiv -\Delta p$, where $\Delta p \equiv p_{\text{ext}} - p_{\text{int}}$ is the difference between the external and internal pressure. Solving the first of Equations (2.4) for τ, and substituting the result into the second equation with $p_t = 0$, we derive a second-order differential equation for the transverse shear tension,

$$\frac{\mathrm{d}}{\mathrm{d}l}\left[\frac{1}{\kappa}\left(\frac{\mathrm{d}q}{\mathrm{d}l} + p_n\right)\right] + \kappa q = 0. \tag{2.5}$$

Performing next a torque balance over an infinitesimal section of the shell, we find

$$q = \frac{\mathrm{d}m}{\mathrm{d}l}. \tag{2.6}$$

To this end, we introduce a linear constitutive equation for the bending moments expressed by the relation

$$m = \kappa_B(\kappa - \kappa_R), \tag{2.7}$$

where κ_B is the bending modulus, and $\kappa_R(l)$ is the curvature of the shell in a resting configuration where the bending moments are assumed to vanish [11]. Justification for Equation (2.7) will be provided in Appendix A. The linear equation (2.7) is expected to be accurate for sufficiently small changes in curvature; when the changes are no longer small, a nonlinear constitutive equation must be employed.

Substituting (2.7) in (2.6), and using the resulting expression to eliminate q from (2.5), we find

$$\frac{\mathrm{d}}{\mathrm{d}l}\left[\frac{1}{\kappa}\left(\frac{\mathrm{d}^2(\kappa-\kappa_R)}{\mathrm{d}l^2}+\frac{p_n}{\kappa_B}\right)\right]+\kappa\frac{\mathrm{d}(\kappa-\kappa_R)}{\mathrm{d}l}=0, \tag{2.8}$$

which can be rearranged into

$$\frac{\mathrm{d}}{\mathrm{d}l}\left[\frac{1}{\kappa}\left(\frac{\mathrm{d}^2(\kappa-\kappa_R)}{\mathrm{d}l^2}+\frac{p_n}{\kappa_B}+\frac{1}{2}\kappa^3\right)\right]-\kappa\frac{\mathrm{d}\kappa_R}{\mathrm{d}l}=0. \tag{2.9}$$

Integrating (2.9) once with respect to l, we derive the integro-differential equation

$$\frac{\mathrm{d}^2\kappa}{\mathrm{d}l^2}=-\frac{1}{2}\kappa(\kappa^2+c)-\frac{p_n}{\kappa_B}+\frac{\mathrm{d}^2\kappa_R}{\mathrm{d}l^2}+\kappa\int_{l_0}^{l}\kappa(l')\frac{\mathrm{d}\kappa_R}{\mathrm{d}l'}\mathrm{d}l', \tag{2.10}$$

where c is an integration constant with dimensions of inverse squared length, and l_0 is an arbitrarily specified arc length.

Using the first of Equations (2.4) in conjunction with Equations (2.6) and (2.7), we find that the in-plane tension is given by

$$\tau=-\frac{1}{2}\kappa_B(\kappa^2+c-2\int_{l_0}^{l}\kappa\frac{\mathrm{d}\kappa_R}{\mathrm{d}l'}\mathrm{d}l'). \tag{2.11}$$

It is important to emphasize that, unlike (2.7), expression (2.11) is *not* a constitutive equation relating the in-plane tension to deformation, but rather expresses an equilibrium condition. An additional constitutive equation may be imposed, and its role will be to determine the total length of the shell and the relative distribution of point particles along the deformed shape with respect to the resting configuration. This distinction has been the source of some confusion in the literature, as will be discussed in Appendix A.

2.2. Open shells

In the case of the open shell depicted in Figure 1(a), physical considerations demand that the bending moments vanish at the two ends,

$$\kappa(x=\pm L)=\kappa_R. \tag{2.12}$$

Equation (2.10) is then to be solved over the half-length $0<l<L$ subject to (2.12) and to the symmetry condition

$$\left(\frac{\mathrm{d}\kappa}{\mathrm{d}l}\right)_{l=0}=0, \tag{2.13}$$

requiring that the curvature reaches an extremum at the mid-point.

The slope angle θ defined in Figure 1(d) is related to the curvature by the equation $\kappa=\mathrm{d}\theta/\mathrm{d}l$. Substituting this expression in the equilibrium equations (2.4) with $p_n=0$ and $p_t=0$, we obtain the first-order differential equations $-\tau+\mathrm{d}q/\mathrm{d}\theta=0$ and $q+\mathrm{d}\tau/\mathrm{d}\theta=0$, which may be combined into the uncoupled second-order equations $\mathrm{d}^2\tau/\mathrm{d}\theta^2+\tau=0$ and $\mathrm{d}^2q/\mathrm{d}\theta^2+q=0$. A solution that respects the global force balance is given by $\tau=-F\cos\theta$ and $q=-F\sin\theta$. Using the torque balance (2.6) along with the constitutive equation (2.7), we find

$$\frac{\mathrm{d}^2\theta}{\mathrm{d}l^2}=-\frac{F}{\kappa_B}\sin\theta+\frac{\mathrm{d}\kappa_R}{\mathrm{d}l}. \tag{2.14}$$

The symmetry condition (2.13) requires that θ vanish at the mid-point, $\theta(l = 0) = 0$, and condition (2.12) requires $\kappa(l = L) = (\mathrm{d}\theta/\mathrm{d}l)(l = \pm L) = \kappa_R$.

Equation (2.14) for the slope angle is an alternative to Equation (2.10) for the curvature. The two formulations have complementary strengths and weaknesses regarding facility for analytical and numerical computation, as will be discussed in Section 3. A generalization of these equations describes the shape of a heavy elastic or a circular shell that is pinned on an inclined plane on one end and is free to roll on the other end [13–15].

2.3. TUBULAR SHELLS

In the case of a closed shell depicted in Figure 1(b), Equation (2.10) or its ancestral Equation (2.8) is to be solved subject to the symmetry condition (2.13) applied at two judiciously chosen points to yield a desired symmetry, as will be discussed in Section 4.

When the resting curvature of the shell is uniform, a formulation in terms of the slope angle θ based on a variational principle yields the nonlinear integrodifferential equation

$$\frac{\mathrm{d}^2\theta}{\mathrm{d}l^2} + p_n \int_{l_0}^{l} \cos[\theta(l) - \theta(l')]\mathrm{d}l' = \gamma \cos(\theta + \delta), \tag{2.15}$$

where γ and δ are two *a priori* unknown constants [16, 17]. Although Equation (2.15) is more cumbersome than its counterpart (2.14) for the open shell, it is nonetheless a useful starting point in theoretical studies of existence of solution.

2.4. SHELL SHAPE IN TERMS OF THE CURVATURE

To compute the shape of the deformed shell in terms of the curvature distribution $\kappa(l)$, we regard the x and y coordinates of point particles along the shell as functions of arc length l, writing $x = x_1(l)$ and $y = x_2(l)$. By definition then, $x_1'^2 + x_2'^2 = 1$, where a prime denotes a derivative with respect to l. Using elementary differential geometry, we derive the relations $\kappa = -x_1''x_2' + x_1'x_2'' = -x_1''/x_2' = x_2''/x_1'$. Next, we introduce the functions $x_3 \equiv x'$ and $x_4 \equiv y'$, and obtain the following system of four nonlinear differential equations,

$$\frac{\mathrm{d}x_1}{\mathrm{d}l} = x_3, \frac{\mathrm{d}x_2}{\mathrm{d}l} = x_4, \frac{\mathrm{d}x_3}{\mathrm{d}l} = -\kappa x_4, \frac{\mathrm{d}x_4}{\mathrm{d}l} = \kappa x_3. \tag{2.16}$$

The initial conditions accompanying this system are $x_1(0) = 0$, $x_2(0) = 0$, $x_3(0) = 1$, and $x_4(0) = 0$, reflecting the choice of the Cartesian axes illustrated in Figures 1(a, b).

3. Flat plates and circular arcs

When the resting curvature of an open shell is uniform, that is, κ_R is independent of l which means that the unstressed shell is either flat or circular, the last two terms on the right-hand side of (2.10) vanish. Setting $p_n = 0$, we obtain the second-order ordinary differential equation

$$\frac{\mathrm{d}^2\kappa}{\mathrm{d}l^2} = -\frac{1}{2}\kappa(\kappa^2 + c). \tag{3.1}$$

Referring to equation (2.11), we set $\tau(l = 0) = -F$ and find $2F = \kappa_B(\kappa_0^2 + c)$, where $\kappa_0 \equiv \kappa(l = 0)$ is the curvature at the mid-point. Eliminating the constant c in favor of the edge force F, we derive the equation

$$\frac{\mathrm{d}^2\kappa}{\mathrm{d}l^2} = -\frac{1}{2}\kappa\left(\kappa^2 - \kappa_0^2 + 2\,\frac{F}{\kappa_B}\right), \tag{3.2}$$

accompanied by the boundary conditions (2.12) and (2.13). Multiplying both sides of (3.2) by $\mathrm{d}\kappa/\mathrm{d}l$, integrating once with respect to l, and enforcing the symmetry condition (2.13), we find

$$\left(\frac{\mathrm{d}\kappa}{\mathrm{d}l}\right)^2 = \frac{1}{4}(\kappa_0^2 - \kappa^2)\left(\frac{4F}{\kappa_B} - \kappa_0^2 + \kappa^2\right). \tag{3.3}$$

Next, we require that the right-hand side of (3.3) is non-negative, and derive the constraint

$$\kappa_0^2 - \frac{4F}{\kappa_B} \le \kappa^2 \le \kappa_0^2. \tag{3.4}$$

Evaluating this inequality at the end of the plate, and rearranging, we find

$$\kappa_R^2 \le \kappa_0^2 \le \kappa_R^2 + \frac{4F}{\kappa_B}, \tag{3.5}$$

which places a bound on the range of variation of the mid-point curvature with respect to the reference value.

We proceed further by assuming that the maximum curvature occurs at the mid-point, and introduce the parametrization

$$\kappa = \kappa_0\,\cos\,\phi, \tag{3.6}$$

where the angle ϕ ranges from 0 at the mid-point to $n\pi - \phi_R$ at the end, n is an integer, and the principal angle ϕ_R is restricted to lie in the range $[0, \pi]$; if the resting shape is flat, $\phi_R = \pi/2$. The dynamic condition at the edges requires $\kappa_R = \kappa_0 \cos(n\pi - \phi_R)$. Substituting the transformation (3.6) in (3.3), we find

$$\left(\frac{\mathrm{d}\phi}{\mathrm{d}l}\right)^2 = \frac{F}{\kappa_B}(1 - \omega_0^2\,\sin^2\,\phi), \tag{3.7}$$

where $\omega_0^2 \equiv \kappa_0^2\kappa_B/(4F)$. Rearranging this definition, we find that the reduced curvature at the mid-point is given by

$$\kappa_0 = \pm 2\omega_0 \hat{F}^{1/2}, \tag{3.8}$$

where $\hat{F} \equiv FL^2/\kappa_B$. Rearranging (3.7), and integrating over half the length of the shell, we obtain

$$\hat{F}^{1/2} = \int_0^{n\pi-\phi_R} \frac{\mathrm{d}\phi}{\sqrt{1 - \omega_0^2 \sin^2\phi}}. \tag{3.9}$$

Expressions (3.8) and (3.9) provide us with a parametric representation for the response diagram, $L\kappa_0$ versus $\hat{F}$, in terms of the dimensionless parameter ω_0 varying in the range $[0, 1]$.

Correspondingly, Equation (2.14) reduces to a well-known equation describing the buckling of an elastica due to a prescribed end-thrust ([3, Section 262])

$$\frac{\mathrm{d}^2\theta}{\mathrm{d}l^2} = -\frac{F}{\kappa_B}\sin\theta, \tag{3.10}$$

accompanied by the symmetry condition $\theta(l=0)=0$ and the requirement $(\mathrm{d}\theta/\mathrm{d}l)(l=L)=\kappa_R$ ensuring that the bending moment vanishes at the end. Multiplying both sides of (3.10) by $\mathrm{d}\theta/\mathrm{d}l$, and integrating once with respect to l, we obtain the first-order nonlinear equation

$$\left(\frac{\mathrm{d}\theta}{\mathrm{d}l}\right)^2 = 2\frac{F}{\kappa_B}(\cos\theta - \cos\alpha) + \kappa_R^2, \tag{3.11}$$

where $\alpha \equiv \theta(l=L)$ is the principal slope angle at the right end, restricted to lie in the range $[0,\pi]$. Applying (3.11) at the mid-point where $\theta=0$, and rearranging, we find

$$\sin^2\frac{\alpha}{2} = \omega_0^2 - \omega_R^2, \tag{3.12}$$

where $\omega_R^2 \equiv \kappa_R^2\kappa_B/(4F)$; for a shell with a flat resting shape, ω_R vanishes. Equation (3.12) provides us with a relationship between the end-slope angle and the mid-point curvature, and requires $\omega_0^2 \le 1+\omega_R^2$, in agreement with (3.5).

To show consistency with the curvature formulation, we rearrange (3.10) and integrate over the length of the plate to find

$$\begin{aligned}\hat{F}^{1/2} &= \frac{1}{\sqrt{2}}\int_0^{n\pi-\alpha}\frac{\mathrm{d}\theta'}{\sqrt{\cos\theta'-\cos\alpha+2\omega_R^2}} \\ &= \frac{1}{2}\int_0^{n\pi-\alpha}\frac{\mathrm{d}\theta'}{\sqrt{\sin^2\dfrac{\alpha}{2}+\omega_R^2-\sin^2\dfrac{\theta'}{2}}} = \frac{1}{2}\int_0^{n\pi-\alpha}\frac{\mathrm{d}\theta'}{\sqrt{\omega_0^2-\sin^2\dfrac{\theta'}{2}}}.\end{aligned} \tag{3.13}$$

When the curvature of the resting shape is sufficiently small, we can introduce the transformation

$$\sin\frac{\theta}{2} = \omega_0\sin\phi, \tag{3.14}$$

and substitute it in the last integral of (3.13) to recover (3.9), thereby reconciling the two formulations.

3.1. FLAT PLATE

When the resting shape of a shell is flat, in which case $\phi_R=\pi/2$ and $\omega_0^2\le 1$, equation (3.9) reduces to

$$\hat{F}^{1/2} = (2n-1)K_c(\omega_0), \tag{3.15}$$

where K_c is the complete elliptic integral of the first kind; expression (3.8) then yields

$$L\kappa_0 = \pm 2(2n-1)\omega_0 K_c(\omega_0). \tag{3.16}$$

To study small deflections, we let ω_0 tend to zero, note that $K_c(0)=\pi/2$, and find the well-known bifurcation points

$$\hat{F} = \alpha_n = (2n-1)^2\frac{\pi^2}{4}. \tag{3.17}$$

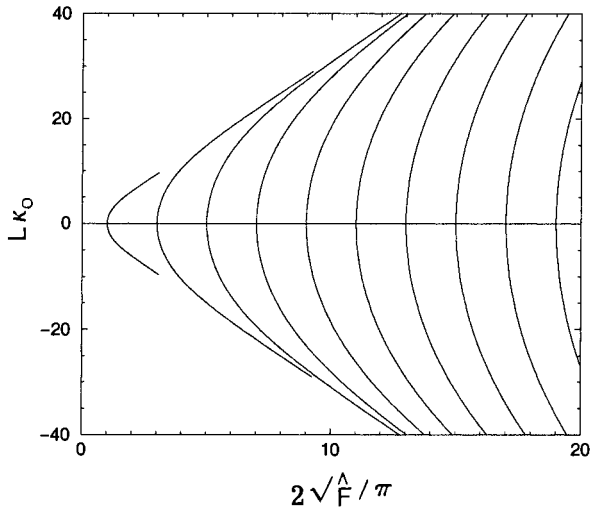

Figure 2. Solution branches for the flat plate: mid-point curvature versus edge force.

Small deflections from the flat shape are thus possible only when the dimensionless force $\hat{F}$ takes one of the critical values α_n. Alternatively, we may linearize the right-hand side of (3.10) and obtain $\mathrm{d}^2\theta/\mathrm{d}l^2 = -(F/\kappa_B)\theta$, whose nontrivial solution is $\theta = A\sin(l\sqrt{F/\kappa_B})$, where A is an arbitrary constant. The boundary condition $\mathrm{d}\theta/\mathrm{d}l = 0$ at the end of the plate is satisfied only when $\hat{F}$ takes one of the values displayed in (3.17).

Figure 2 shows a family of solution branches represented by graphs of the dimensionless mid-point curvature $L\kappa_0$ plotted against the dimensionless force $\hat{F}$ for $n = 1, 2, \ldots, 15$, prepared using the parametric representation provided by (3.15) and (3.16). The results reveal double-point symmetric bifurcations at the critical points given in (3.17).

Figure 3 illustrates a family of buckled shapes corresponding to the first solution branch $n = 1$, for $\omega_0^2 = 0{\cdot}001, 0{\cdot}01, 0{\cdot}02, 0{\cdot}05, 0{\cdot}10, 0{\cdot}20, \ldots, 0{\cdot}9, 0{\cdot}95, 0{\cdot}97, 0{\cdot}99$ and $0{\cdot}999$, corresponding to $2\hat{F}/\pi = 1{\cdot}00025, 1{\cdot}0025, 1{\cdot}0051, 1{\cdot}00129, 1{\cdot}020, 1{\cdot}057, \ldots, 1{\cdot}641, 1{\cdot}852, 2{\cdot}010, 2{\cdot}353$ and $3{\cdot}082$. These shapes were computed by solving Equation (3.2) and then integrating system (2.16) using the fourth-order Runge-Kutta method. The self-intersecting shapes may be identified with deformed half-plates pinned to a horizontal wall on one end, and pulled horizontally toward the pinned point from the other end. In the limit as ω_0 tends to unity, we obtain a flat plate with a mid-point knot.

Love ([3 Section 268]) shows that the simplest family of shapes corresponding to $n = 1$, characterized by the absence of inflection points, is stable, whereas all other shapes corresponding to $n > 1$ are unstable (see also Reiss [18]). Thus, in real life, as the reduced edge force $\hat{F}$ is increased, the plate remains flat until $\hat{F} = \alpha_1$, and then it deforms to obtain the family of shapes displayed in Figure 3.

3.2. Circular arcs

When the resting shape of a plate is curved, the plate deforms as soon as an edge force is applied, however small. As a consequence, the bifurcation points in the solution space displayed in Figure 2 are expected to disappear, which means that the curvature of the resting shape acts as a singular perturbation. This behavior is evident in Thurston's results around

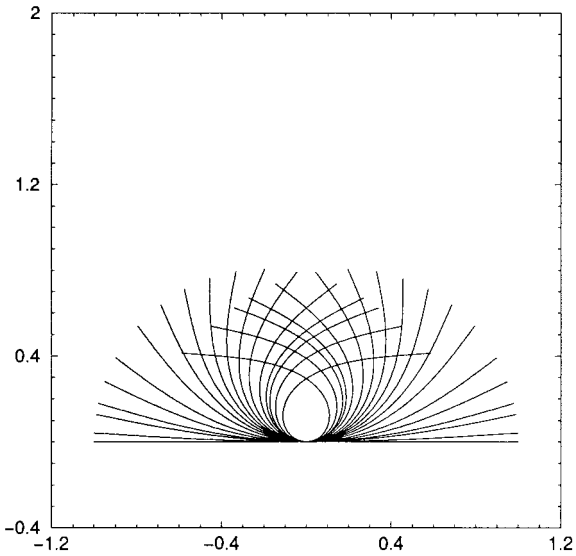

Figure 3. Deformed plate shapes corresponding to the first solution branch $n = 1$ depicted in Figure 2.

the first bifurcation point for a plate whose unstressed shape is a part of a sinusoid [19]; the deviation from the flat shape was regarded as an imperfection from the ideal state.

Instabilities and singular perturbations of bifurcations in the solution space of discrete systems involving interconnected elastic springs were first discussed by Koiter ([25, Chapter 2]). Matkowsky and Reiss [21] presented a physical model consisting of two rigid massless rods connected by a linear torsional spring, which can be considered as the discrete counterpart of a curved plate, and demonstrate that a singular perturbation arises in the solution space of a cubic algebraic equation describing equilibrium. Similar models were discussed by Golubitsky and Schaeffer [22, 23]. A comprehensive review of bifurcation theory as applied to elasticity was given more recently by Antman ([5, Chapter V]).

To show explicitly the overall change of the solution space due to the curvature of the resting configuration, we consider the deformation of a plate whose resting shape is a circular arc with half-aperture angle $\beta\pi$. When $\beta = 0$, the undeformed shell is a flat plate, whereas when $\beta = 0{\cdot}5$, the undeformed shell a semi-circle. Deformed shapes were computed by solving the boundary-value problem expressed by equation (3.2) with accompanying boundary conditions using the shooting method combined with Newton's iterations. The numerical integration of the differential equation was carried out using the fourth-order Runge-Kutta method.

Figure 4 shows solution branches for $\beta = 0{\cdot}1$ and $0{\cdot}5$, the latter corresponding to the semi-circular resting shape. The dashed lines repeat the graphs of Figure 2 for the flat plate, and are included to provide a frame of reference. The numerical results confirm that the bifurcation points disappear, and pairs of solution branches merge to yield closed loops. This behavior is typical of problems exhibiting singular perturbations of break-point bifurcations in the solution space of ordinary and partial differential equations due to asymmetry or other imperfections (*e.g.* [20−24]).

Bifurcation theory suggests that the first upward solution branches displayed in Figure 4 are stable, whereas the first downward branches are stable only up to the vertical turning point; all other solution branches are unstable are thus devoid of a physical meaning ([24, pp.37–38]). Three families of deformed shells with semi-circular resting shape, corresponding to

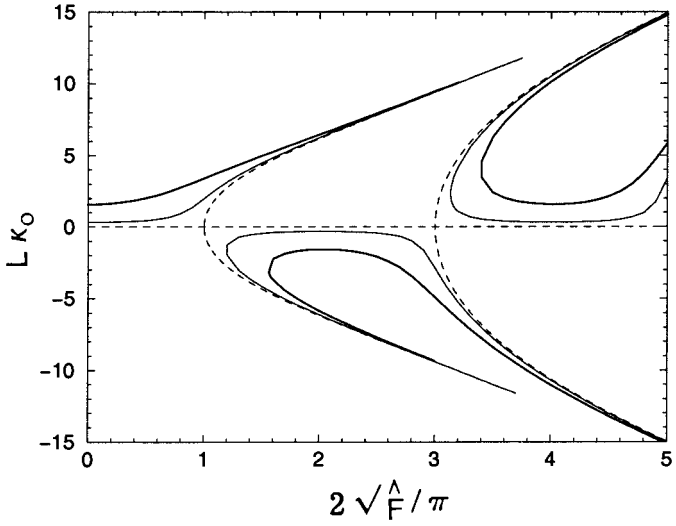

Figure 4. Solution branches for a deformed shell whose resting shape is a circular arc with $\beta = 0{\cdot}1$ (thin solid line) and $0{\cdot}5$ (thick solid line); the dashed lines represent solution branches for the flat plate depicted in Figure 2.

$\beta = 0{\cdot}5$, are shown in Figure 5. The families displayed in Figure 5(a) are stable, whereas those displayed in Figure 5(b) are unstable.

4. Tubular shells

In the second part of our study, we consider the deformation of closed shells illustrated in Figure 1(b), and study equilibrium shapes established as the difference between the external and internal pressure $\Delta p = p_{\text{ext}} - p_{\text{int}}$, equal to the negative of the transmural pressure, is raised from the value of zero corresponding to the resting, but not necessarily unstressed, shape.

4.1. Shells with uniform resting curvature

Suppose that the resting curvature of the shell is uniform, that is, κ_R is independent of arc length l. If the shell is made of a rolled-up elastic sheet, then κ_R vanishes. Setting the last two terms on the right-hand side of (2.10) equal to zero, and recalling that the normal load is given by $p_n = -\Delta p$, we obtain the generalized form of Equation (3.1),

$$\frac{\mathrm{d}^2\kappa}{\mathrm{d}l^2} = -\frac{1}{2}\kappa(\kappa^2 + c) + \frac{\Delta p}{\kappa_B}. \tag{4.1}$$

Equation (4.1) admits an obvious solution corresponding to uniform curvature $\kappa = \kappa_u$ and $c = -\kappa_u^2 + 2\Delta p/(\kappa_B\kappa_u)$. Substituting these expressions in the right-hand side of (2.11), we find the uniform in-plane tension $\tau = -\Delta p/\kappa_u$ expressing the Young–Laplace law.

To describe small deformations from the circular cross-section, we set $\kappa = \kappa_u + \epsilon\kappa'$, where ϵ is a dimensionless number whose magnitude is much less than unity, substitute this expression in (4.1), and linearize with respect to ϵ while holding c constant to find

$$\frac{\mathrm{d}^2\kappa'}{\mathrm{d}l^2} = -\lambda^2\kappa', \tag{4.2}$$

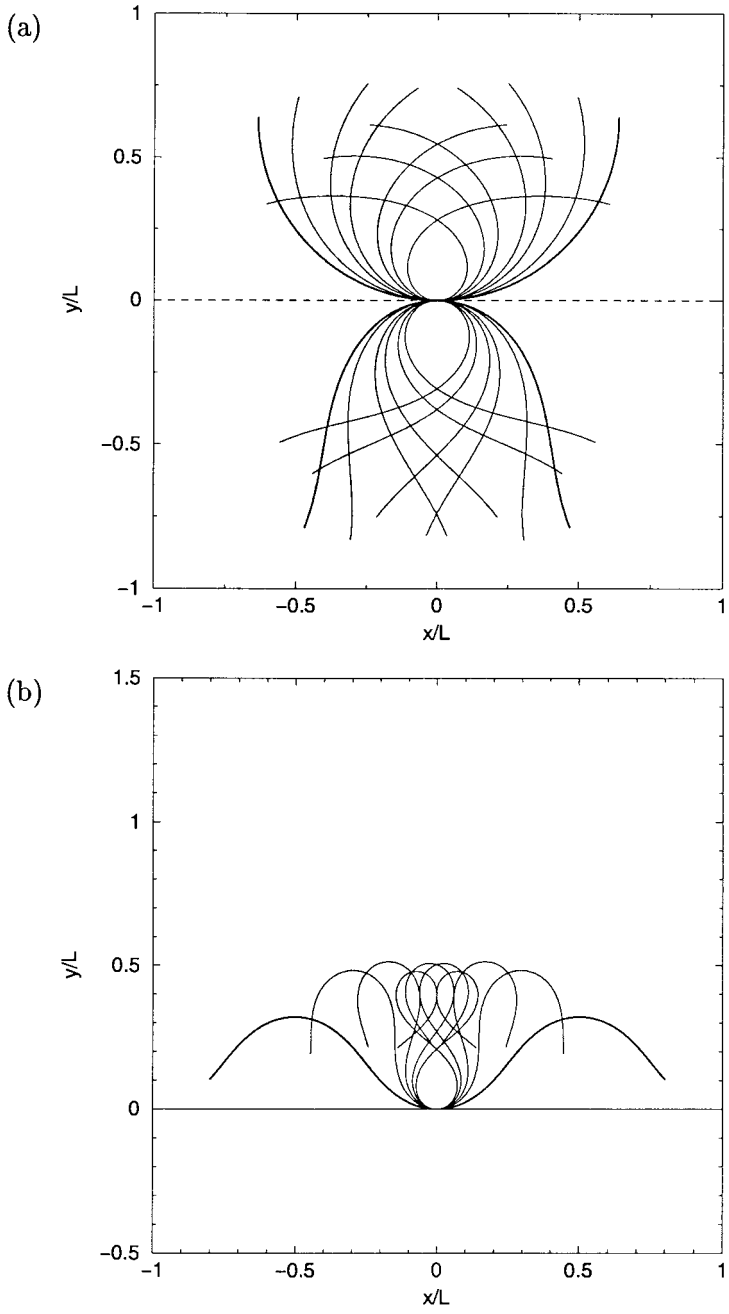

Figure 5. Families of deformed shapes of a shell with semi-circular resting shape. (a) First upward solution branch (stable) for $2\sqrt{\hat{F}}/\pi = 0{\cdot}0$ (thick line), 0·5, 0·8, 1·0, 1·5, 2·0 and 3·2; and first downward solution branch (stable) for $2\sqrt{\hat{F}}/\pi = 1{\cdot}56$ (thick line), 1·6, 1·8, 2·0, 2·5 and 3·0. (b) Second upward solution branch (unstable) for $2\sqrt{\hat{F}}/\pi = 3{\cdot}4$ (thick line), 3·7, 4·0, 4·5 and 5·0.

where we have defined

$$\lambda^2 \equiv \kappa_u^2 + \frac{\Delta p}{\kappa_B \kappa_u}. \tag{4.3}$$

Without loss of generality, we may express the solution of (4.2) in the form $\kappa' = A\cos(\lambda l)$, where A is an arbitrary constant, and require the periodicity condition $\lambda = m\kappa_u$, where m is an integer representing the circumferential mode. Rearranging, we find that small deformations are possible only when the reduced pressure difference takes the values

$$\Delta\hat{p} \equiv \frac{\Delta p}{\kappa_B \kappa_u^3} = \beta_m \equiv m^2 - 1, \tag{4.4}$$

in agreement with classical results on the buckling of cylindrical shells (*e.g.* ([4], [26 p. 177]). Our earlier results for the flat plate suggest that these values correspond to bifurcation points in the solution space.

To compute the shapes of deformed shells, we may work as in Section 3 and convert (4.1) into a first-order equation whose general solution may be expressed in terms of the elliptic cosine function involving two *a priori* unknown scalar parameters [27]. It is more expedient, however, to solve the boundary-value problem expressed by the second-order equation (4.1) using a shooting method, where the trial variables are the reduced curvature at the origin κ_0/κ_u and the integration constant c. For the inextensible shell presently considered, $L = 2\pi/\kappa_u$, where L is the shell perimeter. The objective functions whose simultaneous zeros are desired are

$$f_1(\kappa_0, c) = \kappa(l = L/m) - \kappa_0, \qquad f_2(\kappa_0, c) = \int_0^{L/(2m)} \kappa \,\mathrm{d}l = \frac{\pi}{m}. \tag{4.5}$$

In the numerical implementation of the shooting method, the differential equation was solved using the fourth-order Runge–Kutta method, and the corrections were done using Newton's method. Previous authors have implemented similar procedures to compute families of deformed tube shapes, but did not display the structure of the solution space in terms of a properly defined deflection parameter [16, 17, 28].

Numerical results for the three lowest modes $m = 2$, 3 and 4 are shown in Figure 6. In agreement with small-deflection theory, solution branches emanate from the critical points displayed in (4.4). Each mode is described by an upper solution branch with high curvature and a lower branch with low and possibly negative curvature. The corresponding shapes, however, are identical, with the two conjugate curvatures corresponding to the points of maximum inward and outward radial deflection. Although the stability of the solution branches has not been established, experience suggests that the shell will remain circular until the first critical point $\beta_1 = 3$, and it will them buckle following the first solution branch corresponding to $m = 2$.

Figure 7 displays a family of buckled shapes corresponding to the mode $m = 2$ for $\Delta\hat{p} =$ 3·1, 3·2, 3·3, 3·4, 3·5, 4·0, 4·5, 5·0 and 5·247. As $\Delta\hat{p}$ is increased, the cross-section of the shell becomes elliptical and then biconcave. The dimples of the biconcave disk come into pointwise contact at the critical dimensionless pressure difference $\Delta\hat{p}_{cr} = 5{\cdot}247$, in agreement with the results of previous authors [28].

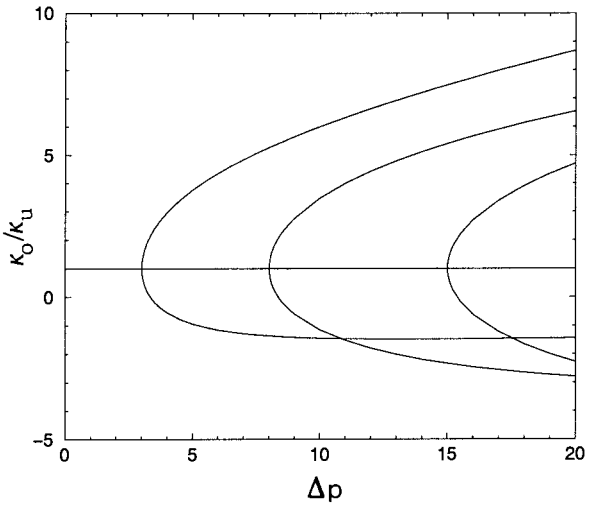

Figure 6. Solution space for a cylindrical shell with circular cross-section, showing the bifurcation of modes $m = 2$, 3, and 4, emanating from the first three critical points $\Delta\hat{p} = \beta_1 = 3$, $\beta_2 = 8$ and $\beta_3 = 15$.

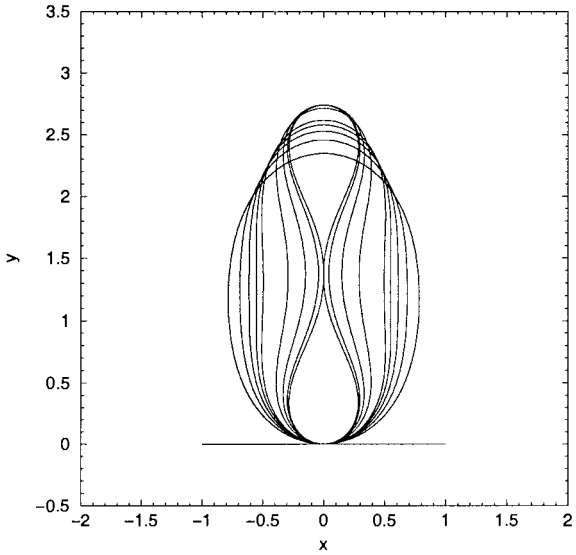

Figure 7. Deformed shapes of a cylindrical tube according to the mode $m = 2$ for $\Delta\hat{p} = 3{\cdot}1$, $3{\cdot}2$, $3{\cdot}3$, $3{\cdot}4$, $3{\cdot}5$, $4{\cdot}0$, $4{\cdot}5$, $5{\cdot}0$ and $5{\cdot}247$ where touching occurs.

4.2. NON-CIRCULAR SHELLS

The solution space illustrated in Figure 6 is similar in structure to that displayed in Figure 2 for the flat plate, in the sense that double-point bifurcations occur at an infinite sequence of critical points β_m. The degeneracy arises because of the axial symmetry of the circular resting shape. Our experience with the curved plate suggests that the non-uniform curvature of the resting shape will cause a singular perturbation in the double-point bifurcations, similar to that discussed in Section 3 for the circular resting plate.

To compute the shape of tubular shells with non-circular resting shapes, we introduce the intermediate function g, decompose Equation (2.9) into the system

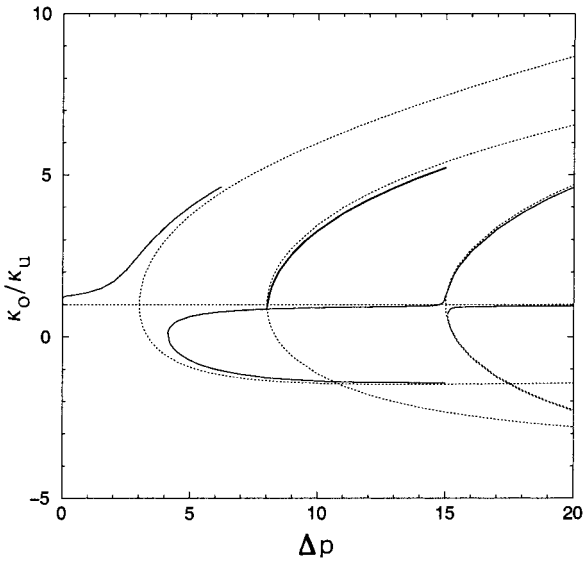

Figure 8. Solution space for a shell with an elliptical-like resting shape corresponding to $s = 2$. The dashed lines represent solution branches of the circular shell for modes m =2, 3 and 4.

$$\frac{\mathrm{d}g}{\mathrm{d}l} = \kappa \frac{\mathrm{d}\kappa_R}{\mathrm{d}l}, \frac{\mathrm{d}^2\kappa}{\mathrm{d}l^2} = \frac{\Delta p}{\kappa_B} - \frac{1}{2}\kappa^3 + \frac{\mathrm{d}^2\kappa_R}{\mathrm{d}l^2} + \kappa g, \tag{4.6}$$

and solve the boundary-value problem using a shooting method similar to that described in Section 4.1, where the trial variables are the values of κ_0/κ_u and $g(0)$. The objective functions are given in Equations (4.5) with c replaced by $g(0)$, and with $m = 1$ to accommodate all shapes.

In the numerical studies, we consider non-circular resting shapes exhibiting s-fold symmetry with respect to arc length. The curvature of the resting shape is described by the equation

$$\kappa_R(l) = \bar{\kappa} + \kappa' \cos(sl\kappa_u), \tag{4.7}$$

where κ_u is the equivalent curvature defined by the equation $L = 2\pi/\kappa_u$, $\bar{\kappa}$ is the arc-length-averaged curvature, κ' is the amplitude of the curvature, and $s = 2, 3, \ldots$. The mode $s = 2$ corresponds to an elliptical-like resting shape.

The solid lines in Figure 8 illustrate the solution space for a shell with an elliptical-like resting shape described by Equation (4.7) with $s = 2$ and $\kappa'/\kappa_u = 0{\cdot}25$. Each one of the displayed solution branches corresponds to a distinct shape. The dotted lines represent the solution space of the circular shell displayed earlier in Figure 6. The break of symmetry due to the non-circular resting shape causes a singular perturbation in the structure of the bifurcation diagram around the resonant critical point $m = s = 2$, similar to that displayed in Figure 4 for a circular plate. The numerical results indicate that the double-point bifurcations are broken at the $m = 2$ mode but not at the $m = 3$ mode. In particular, the broken lower branch of the $m = 2$ mode joins with the upper branch of the $m = 4$ through a nearly horizontal bridge to form a new solution branch from which the $m = 3$ mode emanates. Several previous authors have computed deformed shapes of tubes with elliptical resting shapes, but did not recognize the possibility of multiple solution branches that are likely to be significant for the understanding of the collapse of natural and artificial pulmonary and blood vessels [29–31].

All solution branches, with the exception of the one drawn with the heavy line in Figure 8, display a four-fold subharmonic periodicity with respect to arc length. Figure 9(a) shows a family of cross-sectional shapes corresponding to the first upward branch, for $\Delta\hat{p} = 0$, 1·0, 2·0, 3·0, 3·5, 4·0, 4·5 and 5·0. Figure 9(b, c) shows three possible shapes for $\Delta\hat{p} = 6{\cdot}0$ and 10·0. The compact shape in Figure 9(b) corresponds to the nearly horizontal solution branch which is expected to be unstable. All three shapes displayed in Figure 9(c) are expected to be unstable.

The solid lines in Figure 10 illustrate the solution space for a tube whose resting shape is described by Equation (4.7) with $s = 3$ and $\kappa'/\kappa_u = 0{\cdot}25$. The dashed lines represent the solution branches of the circular shell for modes $m = 2$, 3 and 4. The branches drawn with the dotted lines correspond to shapes that are identical to those of the branches plotted with the solid lines, and have been included to demonstrate consistency with the results for the circular shell. In the case of the $s = 3$ mode, the break of symmetry causes a singular perturbation of the resonant bifurcation point $s = m = 3$. The rest of the bifurcation points seem to be unaffected by the non-uniformity of the reference curvature. Figure 11 shows three possible shapes for $\Delta\hat{p} = 6{\cdot}0$ and 15. The self-intersecting shapes are clearly unphysical, but the smooth shapes are plausible.

5. Flow through a collapsing tube

Consider now steady pressure-driven viscous flow through a collapsing tube whose cross-section changes slowly in the axial direction z, so that the flow may be considered to be locally unidirectional. Subject to this approximation, the axial component of the velocity, u_z, satisfies the parametrically forced Poisson equation

$$\nabla^2 u_z = -\frac{G(z)}{\mu}, \tag{5.1}$$

where $\nabla^2 \equiv \partial^2/\partial x^2 + \partial^2/\partial y^2$ is the Laplacian operator over the tube cross-section, $G(z) \equiv -\mathrm{d}p_{\mathrm{int}}/\mathrm{d}z$ is the negative of the pressure gradient in the streamwise direction inside the tube, and μ is the fluid viscosity. The no-slip boundary condition requires that u_z vanish around the contour of the tube in the xy plane. The flow rate through the tube may be expressed in the form

$$Q \equiv \int u_z \mathrm{d}x\mathrm{d}y = \delta(z)\frac{G\pi a^4}{8\mu}, \tag{5.2}$$

where the integration is over the tube cross-section, δ is the dimensionless hydraulic conductivity coefficient determined by the tube cross-sectional area and shape, $a = L/(2\pi)$ is the equivalent tube radius, and L is the tube perimeter. In the case of a circular tube, a is the tube radius and Poiseuille's law requires $\delta = 1$. Our discussion in Section 4 suggests that the tube contour, and thus δ, is a function of the negative of the transmural pressure $\Delta p \equiv p_{\mathrm{ext}} - p_{\mathrm{int}}$.

Rearranging (5.2), using the definition of G, and assuming that the external pressure is constant, we derive an ordinary differential equation for Δp,

$$\mathrm{d}z = \frac{\pi a^4}{8\mu Q}\delta(z)\,\mathrm{d}\Delta p, \tag{5.3}$$

which may be recast into the dimensionless form

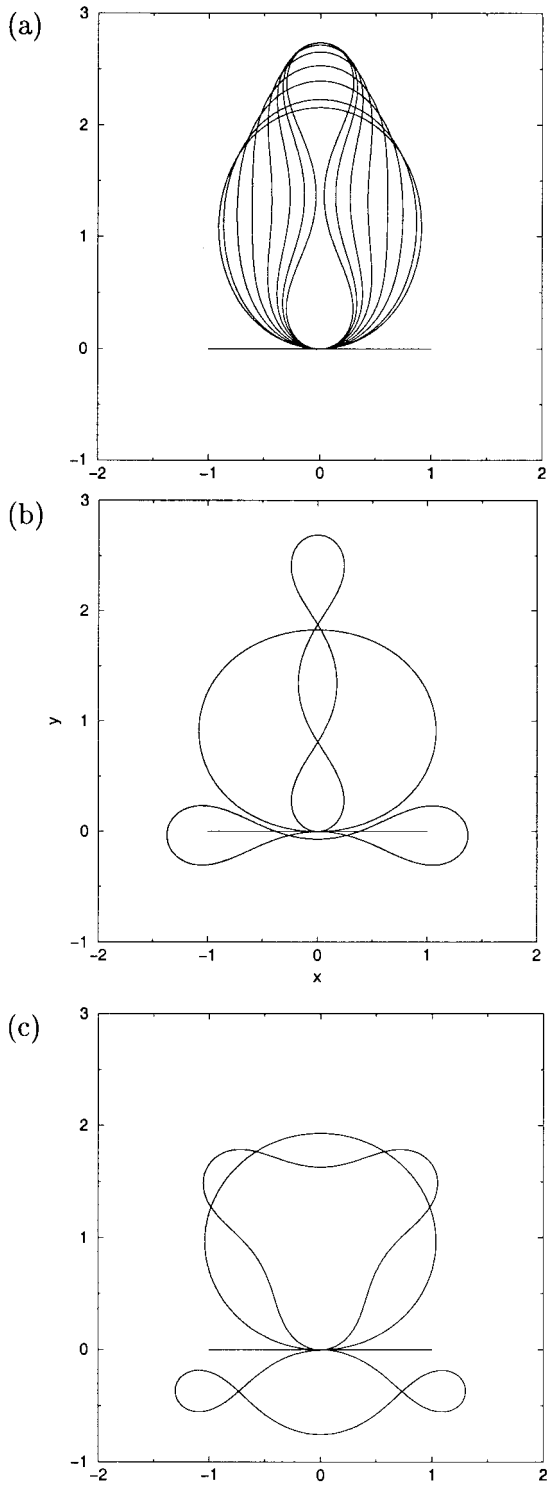

Figure 9. Buckling of a shell with an elliptical-like resting shape corresponding to $s = 2$ and $\kappa'/\kappa_u = 0{\cdot}25$. (a) Deformed shapes along the first upward solution branch displayed in Figure 8. Three possible shapes for (b) $\Delta\hat{p} = 6{\cdot}0$ and (c) $10{\cdot}0$.

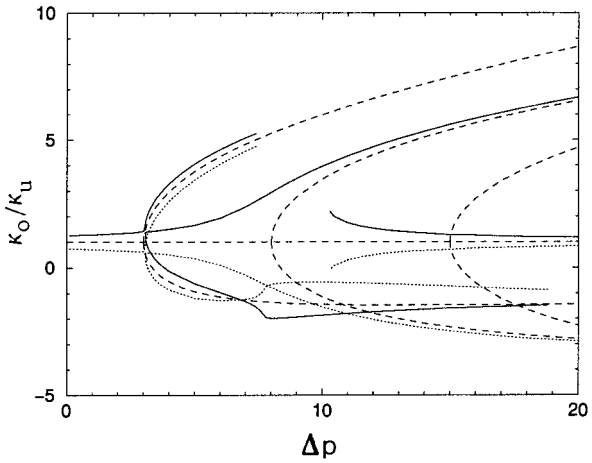

Figure 10. Solution space for a shell with a resting shape corresponding to $s = 3$ and $\kappa'/\kappa_u = 0{\cdot}25$.

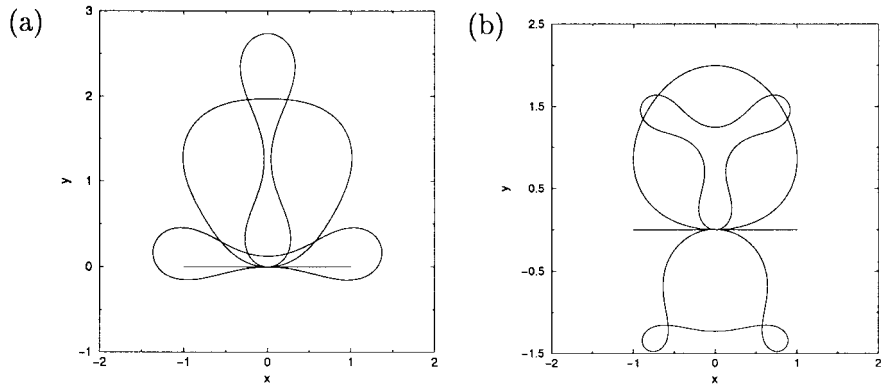

Figure 11. Buckling of a shell with a resting shape corresponding to $s = 3$ and $\kappa'/\kappa_u = 0{\cdot}25$. Three possible shapes for (a) $\Delta\hat{p} = 6{\cdot}0$, and (b) $\Delta\hat{p} = 15{\cdot}0$.

$$\mathrm{d}\hat{z} = \delta(\hat{z})\,\mathrm{d}\Delta\hat{p}, \tag{5.4}$$

where $\hat{z} \equiv z\hat{Q}/a$ is the reduced axial position, and $\hat{Q} \equiv 8\mu Q/(\pi\kappa_B)$ is a dimensionless flow rate. Assuming that the tube starts collapsing at $z = z_0$ where $\Delta\hat{p} = \beta_m$, as shown in Equation (4.4), we may integrate Equation (5.4) to generate the function $\Delta\hat{p}(\hat{z})$ and its inverse. Once this has been accomplished, the three-dimensional shape of a collapsing tube may be reconstructed by stacking adjacent cross-sections next to one another, spacing them by appropriate distances.

Flaherty *et al.* (1972) presented a sketchy graph of the hydraulic conductivity $\delta(\Delta\hat{p})$, but did not discuss the numerical method or the accuracy of their computations [28]. We have reformulated the Poisson Equation (5.1) as an integral equation for the boundary distribution of the shear stress, and then solved it using a boundary element method. The numerical procedure involves decomposing the axial velocity u_z into a particular component v that satisfies the Poisson equation and a homogeneous component f that satisfies Laplace's equation, and then solving for the boundary distribution of the normal derivative of the homogeneous contribution. The end-points of the boundary elements are generated by solving the boundary-value problem discussed in Section 4. Once the boundary distribution of the normal derivative is

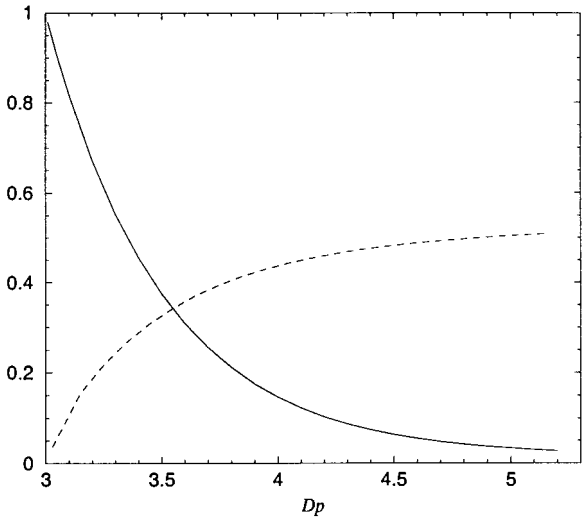

Figure 12. Hydraulic conductivity δ (solid line) and axial position $\hat{z}$ (dashed line) plotted against $\Delta\hat{p}$ for the first solution branch corresponding to $m = 2$, up to the point where touching occurs.

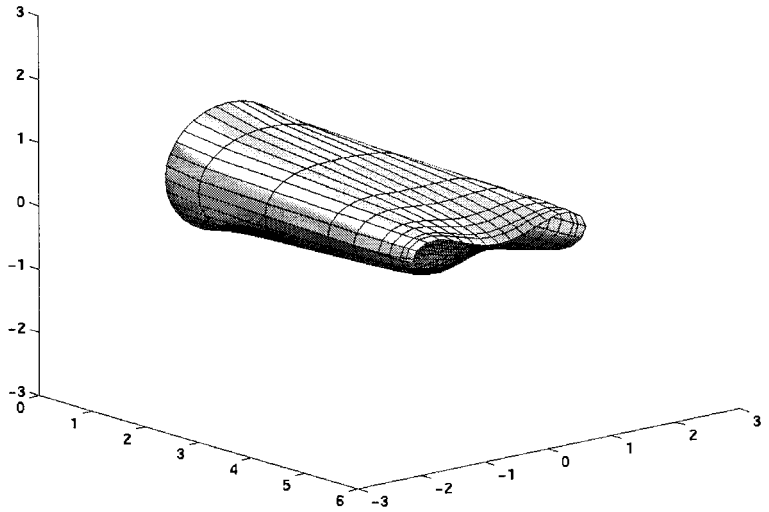

Figure 13. Three-dimensional shape of a collapsing tube reconstructed in terms of two-dimensional cross-sections.

available, the flow rate Q and coefficient δ are computed by evaluating a boundary integral, as discussed in Appendix B. Testing showed that 128 boundary elements around the tube contour are sufficient for obtaining δ accurate to the third significant figure.

The solid line in Figure 12 shows a graph of the dimensionless conductivity δ plotted against $\Delta\hat{p}$ for the first solution branch corresponding to $m = 2$. The line terminates at the point where opposite sections of the tube come into point-wise contact at a critical transmural pressure, as illustrated in Figure 7. The dashed line shows the corresponding axial position $\hat{z}$ generated by integrating Equation (5.4) using a numerical method. The results were used to reconstruct the three-dimensional shape of a collapsing tube in terms of two-dimensional cross-sections, as discussed after Equation (5.4), and the result is shown in Figure 13. This

illustration is similar to that presented by previous authors using more involved finite-element methods [32, 33].

6. Discussion

We have formulated the problem of deflection and post-buckling of elastic plates and tubular elastic shell with arbitrary resting shapes as a combined boundary-value nonlinear eigenvalue problem for the curvature or slope angle, thereby unifying and extending the work of previous authors. Numerical results have demonstrated explicitly that a non-zero or non-uniform resting curvature causes a singular perturbation in the structure of the solution space near bifurcation points, in agreement with theoretical predictions.

We have developed a procedure by which two-dimensional shapes may be stacked together to reconstruct the three-dimensional shape of a slowly collapsing tube carrying a viscous fluid in pressure-driven flow. The assumption of locally unidirectional flow, similar to the boundary-layer approximation, prevents us from taking into consideration boundary conditions imposed at the end of the tube which may be clamped at a rigid junction. To study such configurations, the full three-dimensional problem must be considered.

The numerical methods presented in this paper have been extended to study the buckling and collapse of heavy shells resting on a horizontal or inclined plane. Results of numerical studies will be reported in a future communication.

Acknowledgement

This research has been supported by a grant provided by the National Science Foundation.

Appendix A. Constitative equations for bending moments

In this appendix, we establish a basis for the linear constitutive equation regarding the bending moments, Equation (2.7), in the particular case of inextensible shells whose arc length is locally and globally preserved during the deformation.

Considering first the open shell depicted in Figure 1(a), we introduce the bending-energy functional

$$\begin{aligned} E \;&\equiv \frac{1}{2}\kappa_B \int_{-L}^{L} (\kappa - \kappa_R)^2 \mathrm{d}l + 2Fx(l=L) \\ &= \frac{1}{2}\kappa_B \int_{-L}^{L} \left[\frac{\partial^2 \mathbf{x}}{\partial l^2} \cdot \frac{\partial^2 \mathbf{x}}{\partial l^2} - 2\kappa_R \left(\frac{\partial^2 \mathbf{x}}{\partial l^2} \cdot \frac{\partial^2 \mathbf{x}}{\partial l^2} \right)^{1/2} + \kappa_R^2 \right] \mathrm{d}l + 2F \int_0^L \frac{\mathrm{d}x}{\mathrm{d}l} \mathrm{d}l, \end{aligned} \tag{A1}$$

where $\mathbf{x}$ denotes the position of point particles along the shell, the subscript R signifies the resting state, and the integration is performed along the instantaneous shell shape; the curvature has been expressed in the form $\kappa = |\partial^2 \mathbf{x}/\partial l^2|$. The energy variation due to an infinitesimal virtual displacement $\delta\mathbf{x}$ that preserves the arc length between any two point particles along the shell is given by

$$\delta E = \kappa_B \int_{-L}^{L} \alpha \frac{\partial^2 \mathbf{x}}{\partial l^2} \cdot \frac{\partial^2 \delta \mathbf{x}}{\partial l^2} \mathrm{d}l + F \delta x(l=L), \tag{A2}$$

where $\alpha \equiv 1 - \kappa_R/\kappa$. Integrating (A2) twice, we derive the preferred form

$$\begin{aligned}\delta E = \ & \kappa_B \int_{-L}^{L} \frac{\partial^2}{\partial l^2}\left(\alpha \frac{\partial^2 \mathbf{x}}{\partial l^2}\right) \cdot \delta \mathbf{x}\, \mathrm{d}l \\ & + \kappa_B \left[\alpha \frac{\partial^2 \mathbf{x}}{\partial l^2} \cdot \frac{\partial \delta \mathbf{x}}{\partial l} - \frac{\partial}{\partial l}\left(\alpha \frac{\partial^2 \mathbf{x}}{\partial l^2}\right) \cdot \delta \mathbf{x}\right]_{-L}^{L} + F \delta x(l = L).\end{aligned} \tag{A3}$$

Now, because of the boundary condition (2.12), α vanishes at the two ends, $\alpha(l = \pm L) = 0$, and (A3) simplifies to

$$\delta E = -\kappa_B \int_{-L}^{L} \frac{\partial^2}{\partial l^2}\left[(\kappa - \kappa_R)\mathbf{n}\right] \cdot \delta \mathbf{x}\, \mathrm{d}l + F \delta x(l = L), \tag{A4}$$

which may be recast into the form

$$\delta E = -\kappa_B \int_{-L}^{L} \frac{\partial}{\partial l}\left[\kappa(\kappa - \kappa_R)\mathbf{t} + \frac{\partial(\kappa - \kappa_R)}{\partial l}\mathbf{n}\right] \cdot \delta \mathbf{x}\, \mathrm{d}l + F \delta x(l = L). \tag{A5}$$

The inextensibility condition requires that the virtual displacements are subject to the constraint

$$\mathbf{t} \cdot \frac{\partial \delta \mathbf{x}}{\partial l} = 0, \tag{A6}$$

which suggests the identity

$$\int_{-L}^{L} \frac{\partial}{\partial l}\left[f(l)\mathbf{t}\right] \cdot \delta \mathbf{x}\, \mathrm{d}l = 0, \tag{A7}$$

where $f(l)$ is an arbitrary function.

Now, the principle of virtual displacements provides us with an integral equation of the first kind for the membrane load $\mathbf{p}$,

$$\delta E = \int_{-L}^{L} \mathbf{p} \cdot \delta \mathbf{x}\, \mathrm{d}l + F \delta x(l = L). \tag{A8}$$

Comparing (A8) to (A5), and taking into consideration (A7), we find

$$\mathbf{p} = -\kappa_B \frac{\partial}{\partial l}\left[\left[\kappa(\kappa - \kappa_R) + f(l)\right]\mathbf{t} + \frac{\partial(\kappa - \kappa_R)}{\partial l}\mathbf{n}\right]. \tag{A9}$$

Comparing further (A9) to (2.2) and (2.6), we deduce the linear constitutive for the bending moments m, Equation (2.7). An analogous deduction for the in-plane tension τ is prohibited by the presence of the eigenfunction $f(l)$. Carrying out the differentiation on the right-hand side of (A9), we find that the normal component of the load is given by

$$p_n = \kappa^2(\kappa - \kappa_R) + \kappa f(l) - \frac{\partial^2(\kappa - \kappa_R)}{\partial l^2}. \tag{A10}$$

When the resting curvature vanishes, Equation (A9) takes the simpler form

$$\mathbf{p} = \kappa_B \left[-\frac{\partial}{\partial l}\left[f(l)\frac{\partial \mathbf{x}}{\partial l}\right] + \frac{\partial^4 \mathbf{x}}{\partial l^4}\right]. \tag{A11}$$

Similar results are obtained for the closed shell depicted in Figure 1(b).

Previous authors have used expressions (A9)–(A11) with specific choices for the resting curvature and for the indeterminate function $f(l)$, but did not acknowledge that their choice was arbitrary. Harris and Hearst [34] considered the dynamics of a polymer molecule that develops spring-like forces and bending moments, and assumed that $f(l)$ is a constant, denoted by Λ, playing the role of a Lagrange multiplier. Setting the load $\mathbf{p}$ equal to the rate of change of momentum of an effective distributed molecular mass, they transformed (A11) into an equation of motion for the molecule centerline, and then developed a relation between Λ and the statistical properties of the fluctuating motion. Liverpool and Edwards [35] considered the evolution of a meandering river, set $\kappa_R = 0$ and $f(l) = 0$, and identified the right-hand side of (A10) with with the rate of displacement normal to the centerline. A similar choice was made more recently by Stelitano and Rothman [36] in a numerical study of membrane fluctuations in a viscous medium.

Appendix B. Flow rate along a cylindrical tube with arbitrary cross-section

In this appendix, we develop an expression for the flow rate along a cylindrical tube in terms of the boundary distribution of the shear stress, in pressure-driven flow.

We begin by considering Green's third identity, stating that any two nonsingular functions $f(x, y)$ and $g(x, y)$ satisfy the integral relationship

$$\iint_D (f\nabla^2 g - g\nabla^2 f)\mathrm{d}A = \oint_C \mathbf{n}\cdot(g\nabla f - f\nabla g)\mathrm{d}l, \tag{B1}$$

where C is the boundary of a region D in the xy plane, and $\mathbf{n}$ is the unit vector normal to C pointing inward. Assuming that the function f satisfies Laplace's equation $\nabla^2 f = 0$ and the function g satisfies Poisson's equation $\nabla^2 g = 1$, we derive an expression for the areal integral of f,

$$\iint_D f dA = \oint_C \mathbf{n}\cdot(g\nabla f - f\nabla g)\mathrm{d}l. \tag{B2}$$

One choice for the function g is $g(x, y) = \frac{1}{2}[\alpha(x - x_R)^2 + (1 - \alpha)(y - y_R)^2]$, where α is an arbitrary constant, and (x_R, y_R) are the coordinates of an arbitrary point in the xy plane. This choice with $\alpha = 1/2$ was used in the computations reported in Section 5.

Considering now unidirectional pressure-driven through a cylindrical tube, we decompose the axial velocity u_z into two components as $u_z = f + v$, where f is a harmonic solution satisfying $\nabla^2 f = 0$, v is an inhomogeneous solution satisfying the Poisson equation $\nabla^2 v = -G/\mu$, and G is the negative of the pressure gradient. It will be convenient to set $v(x, y) = -Gg(x, y)/\mu$. The non-slip boundary condition requires $f = -v$ around the tube contour C. Next, we express the inhomogeneous solution as the divergence of a vector function $\mathbf{h}$, writing $v = -(G/\mu)\nabla\cdot\mathbf{h}$. For the particular choice stated at the end of the last paragraph, the scalar components of $\mathbf{h}$ are given by $h_x = \alpha x^3/(6\mu)$ and $h_y = (1 - \alpha)y^3/(6\mu)$.

The axial flow rate through the tube may now be expressed as a boundary integral in the convenient and computationally attractive form

$$Q \equiv \iint_D u_z \mathrm{d}A = \iint_D (f + v)\mathrm{d}A = \oint_C \mathbf{n}\cdot(g\nabla u_z + \frac{G}{\mu}\mathbf{h})\mathrm{d}l. \tag{B3}$$

Once the normal derivative of u_z around the tube is known, the integral on the right-hand side of (B3) may be computed by numerical integration.

References

1. L. Euler, Additamentum I de curvis elasticis, methodus inveniendi lineas curvas maximi monimiui proprietate gaudentes. *Opera Omnia I* 24 (1744) 232–297.
2. T. von Kármán, Festigkeitsprobleme im maschinenbau. *Encyclopädie der Mathematischen Wissenschaften IV/4C* (1910) 311–385.
3. A. E. H. Love, *A Treatise on the Mathematical Theory of Elasticity.* Cambridge: Cambridge University Press (1927). Reprinted by Dover (1944) 643 pp.
4. N. Yamaki, *Elastic Stability of Circular Cylindrical Shells.* Amsterdam: North-Holland (1984) 558 pp.
5. S. S. Antman, *Nonlinear Problems of Elasticity.* Berlin, Heidelberg: Springer Verlag (1995) 750 pp.
6. I. Libai and J. G. Simmonds, *The Nonlinear Theory of Elastic Shells*. Cambridge: Cambridge University Press (1998) 542 pp.
7. T. J. Pedley and X. Y. Luo, Modelling flow and oscillations in collapsible tubes. *Theor. Comp. Fluid Dyn.* 10 (1998) 277–294.
8. C. Pozrikidis, Effect of bending stiffness of the deformation of capsules in simple shear flow. *J. Fluid Mech.* 440 (2001) 269–291.
9. F. Bloom and D. Coffin, *Handbook of Thin Plate Buckling and Postbuckling.* Chapman & Hall / CRC (2000) 786 pp.
10. D. J. Steigmann, Fluid films with curvature elasticity. *Arch. Rat. Mech.* 150 (1999) 127–152.
11. D. J. Steigmann and R. W. Ogden, Plane deformations of elastic solids with intrinsic boundary elasticity. *Proc. R. Soc. London A* 453 (1997) 853–877.
12. D. J. Steigmann and R. W. Ogden, Elastic surface-substrate interactions. *Proc. R. Soc. London A* 455 (1999) 427–474.
13. W. G. Bickley, The heavy elastica. *Phil. Mag. Ser. 7* 17 (1934) 603–622.
14. R. Frisch-Fay, *Flexible Bars.* London: Butterworths (1962) 220 pp.
15. C. Y. Wang, Equilibrium of a heavy, naturally curved sheet on an inclined plane. *ZAMM* 61 (1981) 267–269.
16. I. Tadjbakhsh and F. Odeh, Equilibrium states of elastic rings. *J. Math. Anal. Appl.* 18 (1967) 59–74.
17. I. Tadjbakhsh, Buckled states of elastic rings. In: J. B. Keller and S. Antman (Eds.), *Bifurcation Theory and Nonlinear Eigenvalue Problems*, New York: W. A. Benjamin (1969) pp. 69–92.
18. E. L. Reiss, Column buckling - An elementary example of bifurcation. In: J. B. Keller and S. Antman (Eds.), *Bifurcation Theory and Nonlinear Eigenvalue Problems*. New York: W. A. Benjamin (1969) pp. 1–16.
19. G. A. Thurston, Continuation of Newton's method through bifurcation points. *J. Appl. Mech.* 36 (1969) 425–430.
20. W. T. Koiter, *The Stability of Elastic Equilibrium Behaviour.* Delft University Doctoral Dissertation (1945). Translated into English by W. Titardus, AFFDL-TR-7025 (1970) 306 pp.
21. B. J. Matjowsky and E. L. Reiss, Singular perturbations of bifurcations. *SIAM J. Appl. Math.* 33 (1977) 230–255.
22. M. Golubitsky and D. Schaeffer, A theory for imperfect bifurcation via singularity theory. *Comm. Pure Appl. Math.* 32 (1979) 21–98.
23. M. Golubitsky and D. Schaeffer, *Singularities and Groups in Bifurcation Theory, Volume I*. New York: Springer-Verlag. (1985) 463 pp.
24. G. Iooss and D. D. Joseph, *Elementary Stability and Bifurcation Theory.* Berlin, Heidelberg: Springer-Verlag (1990) 324 pp.
25. W. T. Koiter, *Theory of Elastic Stability and Post-Buckling Behaviour.* Book Manuscript (1962). Translated into English by W. Titardus, 82 pp.
26. Y. C. Fung, *Biodynamics: Circulation.* Berlin, Heidelberg: Springer-Verlag (1984) 404 pp.
27. G. F. Carrier, On the buckling of elastic rings. *J. Math. and Phys.* 26 (1947) 94–103.
28. J. E. Flaherty, J. B. Keller, and S. I. Rubinow, Post-buckling behavior of elastic tubes and rings with opposite sides in contact. *SIAM J. Appl. Math.* 23 (1972) 446–455.
29. E. Kresch and A. Noordergraaf, Cross-sectional shape of collapsible tubes. *Biophys J.* 12 (1972) 274–294.
30. E. Kresch, Compliance of flexible tubes. *J. Biomech* 12 (1979) 825–839.

31. C. Ribrau, S. Naili, M. Bonis, and A. Langlet, Collapse of thin-walled elliptical tubes for high values of major-to-minor axis ratio. *J. Biomech. Eng.* 115 (1993) 432–440.
32. M. Heil and T. J. Pedley, Large post-buckling deformations of cylindrical shells conveying viscous flow. *J. Fluids Struct.* 10 (1996) 565–599.
33. M. Heil, Stokes flow in collapsible tubes: computation and experiment. *J. Fluid Mech.* 353 (1997) 285–312.
34. R. A. Harris and J. E. Hearst, On polymer dynamics. *J. Chem. Phys.* 44 (1966) 2595–2601.
35. T. B. Liverpool and S. F. Edwards, Dynamics of a meandering river. *Phys. Rev. Letters* 75 (1995) 3016–3019.
36. D. Stelitano and D. Rothman, Fluctuations of elastic interfaces in fluids: Theory, lattice-Boltzmann model, and simulation. *Phys. Rev. E* 62 (2000) 6667–6680.